Single π^- Production in n-p Collisions Near Threshold*†

ROBERT HANDLER
The Enrico Fermi Institute for Nuclear Studies and Department of Physics, The University of Chicago, Chicago, Illinois

(Received 9 September 1964; revised manuscript received 4 February 1965)

Over 4000 $n+p \to \pi^-+p+p$ events, obtained in a hydrogen bubble chamber, have been analyzed. The kinetic energies of the initiating neutrons ranged from threshold to 440 MeV. The angular distributions, correlations, and energy partition of the final-state particles as well as the excitation function are presented. They are in excellent agreement with the phenomenological theory of Gell-Mann and Watson, except for the absence in the data of a sharp peak in the momentum partition distribution near the maximum allowed π^- momentum. The Ps amplitudes account for less than 1% of the total cross section. The intensities of the various types of transitions are determined. Examples of sets of amplitudes which yield these intensities are given. However, a large number of amplitudes contribute to the cross section, and the ambiguities are too great to allow evaluation of individual amplitudes.

INTRODUCTION

THE experimental study of inelastic nucleon-nucleon scattering near the threshold for single-pion production has concentrated on the channels

$$p+p \to n+p+\pi^+, \quad \sigma=\sigma_{11}+\sigma_{10}, \tag{1a}$$

$$p+p \to d+\pi^+, \quad \sigma=\sigma_{10}', \tag{1b}$$

$$p+p \to \pi^0+p+p, \quad \sigma=\sigma_{11}, \tag{1c}$$

in which the initial state is a two-proton system.[1-3] The notation for the σ's after each reaction is that of Gell-Mann and Watson.[4] σ_{if} is the cross section for transitions between pure initial and final isotopic spin states of the two nucleons. Primes on the σ's indicate a bound final two-nucleon state. The neutron-proton reactions

$$n+p \to \pi^-+p+p, \quad \sigma=\tfrac{1}{2}(\sigma_{01}+\sigma_{11}), \tag{2a}$$

$$n+p \to \pi^0+d, \quad \sigma=\tfrac{1}{2}\sigma_{10}', \tag{2b}$$

$$n+p \to \pi^0+n+p, \quad \sigma=\tfrac{1}{2}(\sigma_{01}+\sigma_{10}), \tag{2c}$$

$$n+p \to \pi^+ +n+n, \quad \sigma=\tfrac{1}{2}(\sigma_{01}+\sigma_{11}), \tag{2d}$$

are difficult to investigate. Available neutron beams have low intensity and large energy spreads. If bound neutrons provide the target, the basic process is distorted. Moreover, in (2b) and (2c) it is difficult to measure the π^0 momentum, and in (2a) and (2d) the cross sections are small.

The experiment described in this paper is a detailed study of 4079 hydrogen bubble-chamber events of type (2a). It was undertaken to examine the differential form of σ_{01}, about which little is known, and also that of σ_{11}. (2a), (2c), and (2d) depend on σ_{01} but (2c) is dominated by the strong σ_{10} term. Reaction (2a) is unique in this series in that its final state consists entirely of charged particles, thus making it ideal for study with a visual detector where each event, apart from spin orientations, can be described completely. A small hydrogen bubble chamber in a high magnetic field was the instrument used for the investigation. It might be thought that this would be inappropriate for reaction (2a) with a cross section of about 50 μb, corresponding to a mean free path of 30 000 chamber diameters, since no more than about 20 tracks can be tolerated in satisfactory bubble-chamber operation. However, in a neutron beam these tracks are all secondaries, and it is only the ratio of their cross section to (2a) that is important. Moreover, the secondaries from neutron-proton scattering in the hydrogen are useful. These recoils were used to find the energy spectrum of the neutron beam and with it the excitation function of (2a).

THEORY

Form of the Transition Probability

According to the analysis of Gell-Mann and Watson[4] reaction (2a) is governed by two isotopic spin amplitudes a_{11} and a_{01}. These will be referred to as the $I=1$ and the $I=0$ transitions, respectively. To specify these amplitudes in more detail, a notation defining the kinematics is needed. Figure 1 represents an example of the final state in the center-of-mass system. $\mathbf{Q}$ is the π^- momentum; $\mathbf{q}$ and $\mathbf{q}'$ are the momenta of the

* Submitted as a thesis to the Department of Physics of the University of Chicago in partial fulfillment of requirements for the PhD degree.

† Research supported by a joint program of the U. S. Office of Naval Research and the National Science Foundation.

[1] R. L. McIlwain, K. J. Deahl, M. Derrick, J. E. Fetkovich, and T. H. Fields, Phys. Rev. **127**, 239 (1962); R. H. March, *ibid.* **120**, 1874 (1960); L. G. Pondrom, *ibid.* **114**, 1623 (1959); T. H. Fields, J. G. Fox, J. A. Kane, R. A. Stallwood, and R. B. Sutton, *ibid.* **109**, 1713 (1958); R. A. Stallwood, T. H. Fields, J. G. Fox, and J. A. Kane, Bull. Am. Phys. Soc. **1**, 71 (1956); R. H. Hildebrand, Glasgow Conference Report, 1954, p. 245 (unpublished).

[2] T. H. Fields, J. G. Fox, J. A. Kane, R. A. Stallwood, and R. B. Sutton, Phys. Rev. **109**, 1704 (1958); T. H. Fields, J. G. Fox, J. A. Kane, R. A. Stallwood, and R. B. Sutton, *ibid.* **95**, 684 (1954); F. S. Crawford and M. L. Stevenson, Lawrence Radiation Laboratory Report Nos. UCRL 2187, 2188, 1953 (unpublished).

[3] (a) C. York, R. March, W. Kernan, and J. Fisher, Phys. Rev. **113**, 1339 (1959); (b) R. A. Stallwood, R. B. Sutton, T. H. Fields, J. G. Fox, J. A. Kane, *ibid.* **109**, 1717 (1958); (c) B. J. Moyer and R. K. Squire, *ibid.* **107**, 283 (1957); (d) A. F. Dunaĭtsev and Y. D. Prokoshkin, Zh. Eksperim. i Teor. Fiz. **36**, 1656 (1959) [English transl.: Soviet Phys.—JETP **9**, 1179 (1959)]; (e) J. W. Mather and F. A. Martinelli, Phys. Rev. **92**, 780 (1953).

[4] M. Gell-Mann and K. M. Watson, Ann. Rev. Nucl. Sci. 4, 219 (1954). A. H. Rosenfeld, Phys. Rev. **96**, 139 (1954).

TABLE I. Allowed transitions.[a]

Type	Initial state	Final state	Isospin	Parity	Transition amplitude
Ss	$^3P_0$	$^1S_0s_0$	1	−	ah
Sp	$^3S_1$	$^1S_0p_1$	0	+	$b_1{}^0hQ$
	$^3D_1$	$^1S_0p_1$	0	+	$b_2{}^0hQ$
Ps	$^1S_0$	$^3P_0s_0$	1	+	c_1P
	$^1D_2$	$^3P_2s_2$	1	+	c_2P
	$^3S_1$	$^3P_1s_1$	0	+	$c_1{}^0P$
	$^3D_1$	$^3P_1s_1$	0	+	$c_2{}^0P$
	$^3D_2$	$^3P_2s_2$	0	+	$c_3{}^0P$
Pp	$^3P_0$	$^3P_1p_0$	1	−	$d_{10}PQ$
	$^3P_1$	$^3P_0p_1$	1	−	$d_{01}PQ$
	$^3P_1$	$^3P_1p_1$	1	−	$d_{11}PQ$
	$^3P_1$	$^3P_2p_1$	1	−	$d_{21}PQ$
	$^3P_2$	$^3P_1p_2$	1	−	$d_{12}PQ$
	$^3P_2$	$^3P_2p_2$	1	−	$d_{22}PQ$
	$^1P_1$	$^3P_0p_1$	0	−	$d_0{}^0PQ$
	$^1P_1$	$^3P_1p_1$	0	−	$d_1{}^0PQ$
	$^1P_1$	$^3P_2p_1$	0	−	$d_2{}^0PQ$

[a] $P=|\mathbf{P}|$; $Q=|\mathbf{Q}|$.

two protons. $\hat{N}$ is a unit vector in the direction of the incoming neutron and $\mathbf{P}=\mathbf{q}-\mathbf{q}'$.

The final three-body state can be described in terms of quantum numbers S, L, j, l, J. The spins of the two protons couple to form $\mathbf{S}$ (eigenfunction χ_s). $\mathbf{L}$, the relative angular momentum of the two-proton system [eigenfunctions $Y_L(\mathbf{P})$] couples with $\mathbf{S}$ to form an intermediate angular momentum $\mathbf{j}$, and finally $\mathbf{j}$ couples with $\mathbf{l}$, the angular momentum associated with relative motion of the π^- with respect to the center of mass of the two-proton system [eigenfunctions $Y_l(\mathbf{Q})$] to form a total angular momentum $\mathbf{J}$. The notation defining the final state is of the form $^{2S+1}L_jl_J$ (e.g., $^3P_2p_2$, $^1S_0p_1$).

According to Gell-Mann and Watson,[4] the following assumptions should be valid near threshold:

(a) Owing to the short range of the interaction, only states for which L and l are 0 or 1 contribute appreciably to the cross section.

(b) Except for final-state interactions, the momentum dependence of the various final-state partial waves is determined by phase space alone.

(c) The only significant final-state interaction is that between the two nucleons when they are in a relative S state.

A further assumption made in this paper is the neglect of all incoming waves other than s, p, and d. Table I is a listing of allowable transitions of class A for these incoming waves. Column 6 contains the momentum dependence of the various states. The factor h, a function of P alone, has been inserted to describe the effect of the $^1S_0$ p-p interaction. The detailed nature of h will be discussed later. Figure 2 shows a graph of h^2 as a function of P.

For an unpolarized neutron beam in the direction $\hat{N}$, the distribution of particles in the final states can

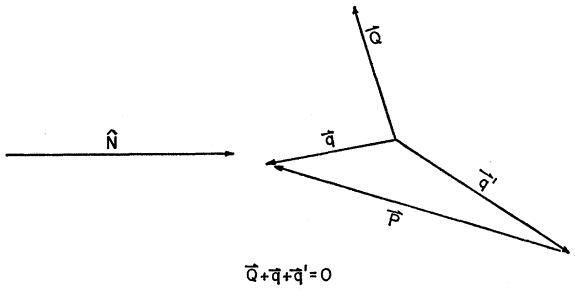

FIG. 1. Momentum vectors describing an event in the center of mass.

be described in terms of P, Q, and angle variables

$$\mu_P=\cos(\mathbf{P},\hat{N}),$$
$$\mu_Q=\cos(\mathbf{Q},\hat{N}),$$
$$\mu=\cos(\mathbf{P},\mathbf{Q}).$$

The absolute squares of the matrix elements summed over final and averaged over initial m states for the four types of outgoing waves are as follows:

$$f_{Pp}=P^2Q^2[\alpha_1+\alpha_2\mu_P{}^2+\alpha_3\mu_Q{}^2+\alpha_4\mu^2+\alpha_5\mu\mu_P\mu_Q], \quad (3a)$$

$$f_{Ps}=P^2[\beta_1+\beta_2\mu_P{}^2], \quad (3b)$$

$$f_{Sp}=h^2Q^2[\gamma_1+\gamma_2\mu_Q{}^2], \quad (3c)$$

$$f_{Ss}=h^2[\delta_1]. \quad (3d)$$

These follow from a standard application of the rules governing addition of angular momenta. Interference between the Ps $I=0$ and the Pp $I=1$ states and interference between the Ps $I=1$ and the Pp $I=0$ states will lead to terms of the form

$$f_{PsPp}=P^2Q[c_1\mu_Q+c_2\mu_P{}^2\mu_Q+c_3\mu\mu_P] \quad (3e)$$

and finally interference between outgoing Sp $I=0$ and Ss $I=1$ states will lead to a term of the form

$$f_{SpSs}=h^2Q[d_1\mu_Q]. \quad (3f)$$

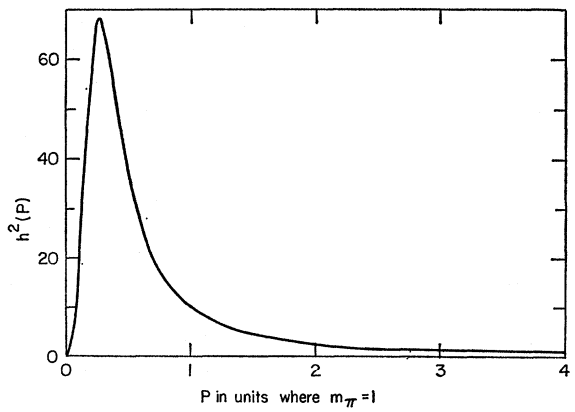

FIG. 2. $^1S_0$ final-state factor $h^2(P)$ versus P.

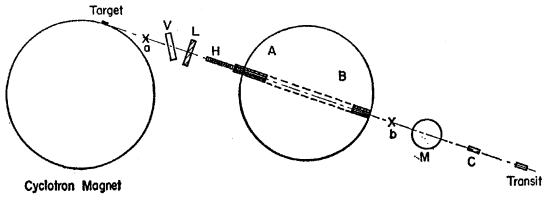

FIG. 3. Neutron-beam geometry and collimation.

These are the only terms present in the total transition probability

$$f=f_{Pp}+f_{Ps}+f_{Sp}+f_{Ss}+f_{PsPp}+f_{SpSs}$$

if conditions (A), (B), and (C) are valid. Note that the interference terms have the property of changing sign under the transformation $\mathbf{Q}\rightarrow-\mathbf{Q}$ ($\mu_Q\rightarrow-\mu_Q$, $\mu\rightarrow-\mu$), whereas the other terms are invariant under this transformation.

$^1S_0$ p-p Final-State Interaction

To calculate $h(P)$, the $^1S_0$ proton-proton interaction was assumed to be described by a potential $V(r)$ of the form

$$V=+\infty;\quad 0\leq r\leq r_c,$$
$$V=-V_0;\quad r_c\leq r\leq r_0,$$
$$V=e^2/r;\quad r>r_0.$$

V_0 and r_0 were set to give the correct $^1S_0$ scattering length and effective range for $r_c=0.355$ (in units in which the pion mass $m_\pi=1$). The value of h appropriate to the above interaction, is $h=\psi_i(r_c)/\psi_0(r_c)$, where ψ_i is the S-wave solution to Schrödinger's equation for the above potential and ψ_0 is the S-wave solution for V everywhere 0. $h^2(P)$ is shown in Fig. 2.

Effect of 3-3 Resonance

Mandelstam[5] has developed a resonance theory applicable to single-pion production in energy regions where the cross section is dominated by the 3-3 resonance. While this experiment was done with a neutron beam of energy $\leq$450 MeV, considerably below the energy necessary for the reaction $N+N\rightarrow N^*+N$, it would be interesting to see how much of the near-threshold behavior can be attributed to the broad resonance.

Mandelstam's theory assumes that all π production takes place through states in which the π is in an $I=\frac{3}{2}$ state with respect to one nucleon. This has the immediate effect of forbidding the $I=1$ transition $^3P_0\rightarrow{}^1S_0s_0$ and all $I=0$ transitions. These transitions, however, are the only ones favored by the nucleon-nucleon final state interaction in Table I. It is clear that any attempt to apply Mandelstam's theory near to threshold should include the transitions

$$^3P_0\rightarrow{}^1S_0s_0,$$
$$^3S_1\rightarrow{}^1S_0p_1,$$
$$^3D_1\rightarrow{}^1S_0p_1,$$

in addition to those Mandelstam uses in his theory. Since Mandelstam's states are defined by a different coupling scheme, this is a rather extensive job and it was felt best to treat it in a separate paper. The present paper will therefore only include comparisons with the theory of Gell-Mann and Watson.

[5] S. Mandelstam, Proc. Roy. Soc. (London) **A244**, 491 (1958).

EXPERIMENT

Beam

Figure 3 shows the beam setup. The circulating proton beam of the 450-MeV Chicago synchrocyclotron struck a $\frac{1}{4}$-in.$\times\frac{1}{4}$-in. Be target located on a 76-in. radius orbit. Neutrons produced forward with respect to this circulating beam passed through a gate valve V, a 1-in. slab of lead L, two collimators A and B resting in a 6-in. hole in the rotary shield S, a magnet M, and finally a 9-in. liquid-hydrogen bubble chamber C. The

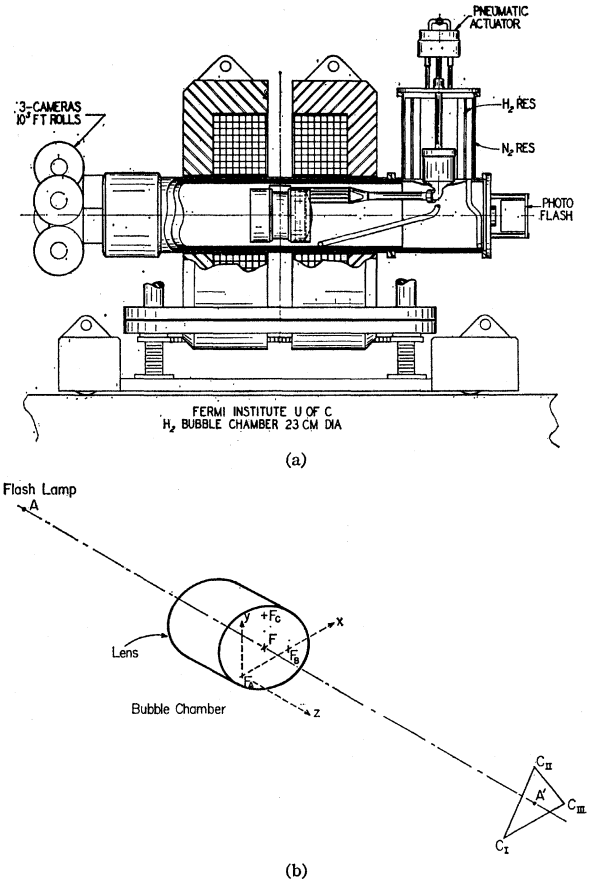

FIG. 4. (a) Bubble chamber in its magnet. (b) Schematic diagram of bubble-chamber optical system.

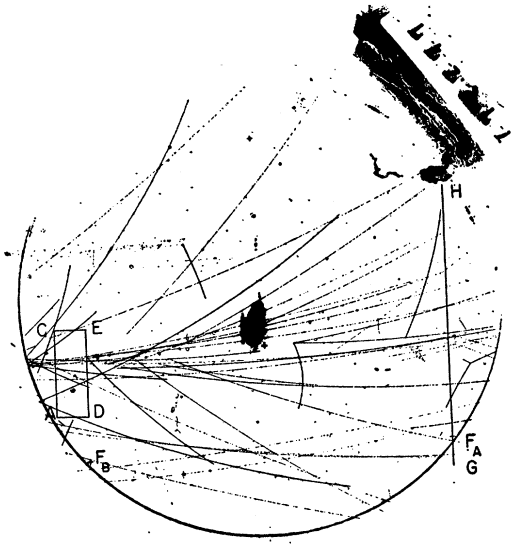

FIG. 5. Photograph from view II of an event. Recoil protons from the wall and from the hydrogen are evident.

lead slab eliminated most of the γ-ray component of the beam; the collimators defined the beam to a small angle and the magnet was used to deflect any charged component. Collimators A and B were lead cylinders 6 in. in diameter. A was 3 ft long and had a $\frac{1}{2}$-in. hole along its axis. B was $1\frac{1}{2}$ ft long and had a $\frac{3}{4}$-in. axial hole. In addition, a 1-m long $\frac{1}{2}$-in. diameter thin-walled stainless-steel pipe H filled with paraffin was inserted into the hole in A to harden the beam by scattering out low-energy ($\lesssim$100 MeV) neutrons.

The beam was aligned as follows:

The shield S was rotated until the line *ab* was tangent to the 76-in. cyclotron orbit circle. A transit in the experimental area was sighted along line *ab* and the target moved on the 76-in. orbit circle until it appeared in the center of the transit field of view. The transit was then locked in place and used to determine the beam line in the experimental area.

Bubble Chamber

Figure 4(a) is a drawing of the hydrogen bubble chamber and its magnet. This magnet maintained the chamber in a field of 24.3$\pm$0.2 kG uniform within $\frac{1}{2}$% over the illuminated volume of the chamber. The magnet was positioned so that the beam line bisected the 2-in. gap and passed roughly through the center of the chamber.

The elements of the bubble chamber with its associated optics, important for the description of this experiment, are shown schematically in Fig. 4(b). The bubble chamber is a 9-in. diameter stainless-steel cylinder 6 in. deep. The ends are closed by two parallel glass windows perpendicular to the chamber axis AA'. Light from a flash tube at A is brought to a focus at A' in the plane of the camera lens by a single 10-in. plano-convex lens placed just outside the chamber on the A side. The reference coordinate system is established by three fiducial crosses etched on the inside of the window adjacent to A'. These crosses F_A, F_B, and F_C form an equilateral triangle. There is a fourth cross F at the centroid of this triangle. Three camera lenses are mounted at the vertices of the equilateral triangle C_{I} C_{II} C_{III} on a plate passing through A'. In the cryostat construction, this plate is rigidly connected to the vacuum window and sealed to the rest of the system in a spherical seat. The camera plate can be moved parallel to itself in two directions. In the optical alignment, a telescope with an illuminated reticle is mounted at the centroid of C_{I} C_{II} C_{III} with its axis perpendicular to the plate. The camera plate is moved via the spherical seal until it is parallel to the front bubble-chamber window, then translated until the telescope cross hair coincides with the image of F and finally rotated about the axis AA' to a point where F_AF_B is parallel to C_{I} C_{III}. The right-handed coordinate system used in the data reduction routine has its origin at F_A, positive x axis along F_AF_B, and z axis parallel to AA'. The cameras are mounted so that the film is parallel to, and the lens axes are all perpendicular to, the lens plate. The neutron beam in this experiment passed near to the center of the chamber in a direction close to the negative x axis of the fiducial coordinates.

The beam intensity was set for approximately 15 elastic proton recoils per picture. Figure 5 is a photograph showing the fiducial crosses F_A, F_B, and F_C, some recoil protons from the wall of the chamber and from the hydrogen, and a π^- production event. Altogether 338 500 sets of three stereographic pictures were taken of which 296 000 were of acceptable quality for scanning.

Scanning Procedure

1. π^- Events

All usable film was scanned twice. Comparing results from the same film by different scanners showed that the average efficiency exceeded 96%. Except for possible systematic biases, this implies a double scan efficiency of over 99.8%. All frames said to contain π^- events ($n+p \rightarrow p+p+\pi^-$) were checked for authenticity. By correlating the track density, and angular and curvature information contained in a picture, a knowledgeable observer could separate π^- events from all possible background in over 99% of the frames checked.

In order to check for a systematic bias against seeing a particular configuration, all frames which were listed by only one of the two scanners (singles) were examined. These singles were 12.7% of the total number of events listed. Of these 48% contained no valid event. The

remaining 52% could be broken into roughly four categories:

(a) 32%—events which occurred in a region of very high background. This does not represent a bias against a particular configuration, but could cut the over-all scanning efficiency.

(b) 23%—the π^- track was short and difficult to see.

(c) 10%—the tracks of the two protons were nearly superimposed on each other.

(d) 35%—clearly visible events which were hard to miss. Probably the bulk of these events were seen by both scanners, but one of them recorded the frame number incorrectly.

Error type (d) is clearly one which will be randomly distributed about the events, and the chance of two scanners making a frame number error on the same frame is indeed small. The seriousness of error types (b) and (c) can be estimated by seeing how many of these types were seen by both scanners. It was found that the average scanning efficiency for type (b) events was 89% and 94.5% for events of type (c). The double scanning efficiency, then, for both types (b) and (c) was probably in excess of 98.5% and can, for all practical purposes be considered 100%.

Let $\mathbf{r}_0$ be the vertex (singular point) of a π^- event. All events for which $x_0<+1$ cm were discarded as being too short for accurate measurement or positive identification. The density of singular points as a function of x_0 in the region $1\leq x\leq 17$ can be fitted by a constant distribution with a χ^2 of 10 (expected 16). Thus, there is no statistically significant variation of scanning efficiency with x_0. The background, however, is much higher near the upstream chamber wall than in the center or downstream region, due to the large number of recoil protons which emerge from the wall of the chamber. The magnetic field tends to sweep these protons out of the beam line and by the center of the chamber the background density is only about half of what it is in the upstream region. This shows the scanning efficiency was not a function of background.

Altogether 5208 π^- events were found and checked. As a consequence of the above considerations, it was felt that there were no significant systematic scanning biases or errors.

2. *Recoil Events*

The reaction $n+p\rightarrow n+p$ was used to monitor the neutron beam both as to intensity and energy distribution. Many such elastic recoil protons can be seen in Fig. 5. The energy of the incoming neutron is determined by a measurement of the recoil proton momentum if the neutron direction is known. The momentum of the recoils can be most accurately measured for very long tracks. For this reason, it was decided to scan the film for recoil proton tracks starting in the region $ACDE$ and ending past the line GF_AH in view II (see Fig. 5).

In all, 3.3% of the pictures, uniformly distributed throughout the film were scanned for such "recoil events" by one scanner who found 3081 of them. The efficiency for finding these recoils was determined by checking 14% of this scanned film, and the results in computing the intensity were scaled to unit efficiency. It was found that there existed a 3% background due to the reaction

$$n+p\rightarrow\pi^0+d.$$

These events were subtracted from the total number found. After all corrections were made, it was estimated that there were 3350 ($\pm 9\%$) recoil events in 3.3% of the film. The 9% error is due to statistics, uncertainty in scanning efficiency, and events which start so near to lines AC or DE that it could not be decided whether they were inside $ACDE$ or not.

DATA REDUCTION

Measurement

The three stereo views of each event were projected in turn at twice life-size on a measuring table. This table is equipped with a fine cross hair movable in two dimensions and linked to encoders that record on paper tape. The number of bits corresponding to the full range in both the x and y directions is 10 000. In measuring an event, the operator superimposes the cross hair on the images of the F_A and F_B fiducial marks, the singular point, and three other points along each track. The cross hair coordinates are punched on paper tape (via a foot switch) at each superposition and the procedure is repeated for each view.

Track Analysis

Physically, a π^- event is completely specified when the coordinate $\mathbf{r}_0$ of the singular point, the three-momentum vectors ($\mathbf{P}_1$ and $\mathbf{P}_2$ of the two protons and $\mathbf{P}_\pi$ of the π^- meson) of the final-state particles and the momentum $\mathbf{P}_n$ of the incident neutron are known. The twelve components of $\mathbf{P}_1$, $\mathbf{P}_2$, $\mathbf{P}_\pi$, and $\mathbf{P}_n$ are not independent but are constrained to obey the four conservation equations of momentum and energy:

$$\mathbf{P}_n=\mathbf{P}_1+\mathbf{P}_2+\mathbf{P}_\pi,$$
$$(M_n^2+P_n^2)^{1/2}=(M^2+P_1^2)^{1/2}+(M^2+P_2^2)^{1/2}+(m_\pi^2+P_\pi^2)^{1/2}$$

(M_n=neutron mass, M=proton mass, $m_\pi=\pi^-$ mass). Thus, if nothing is known about $\mathbf{P}_n$, the eight independent parameters $\mathbf{P}_1$, $\mathbf{P}_\pi$, P_{2y}, and P_{2z} can be used along with $\mathbf{r}_0$ to completely specify the event. If the direction of $\mathbf{P}_n$ is known but not its magnitude the singular point plus six independent parameters, such as $\mathbf{P}_1$ and $\mathbf{P}_\pi$, specify the event.

The function of the analyzing program is to construct an event in space, determined by $\mathbf{r}_0$ and the independent momentum variables, corresponding to the points measured on the three stereo projections of this event. The singular point's coordinates in space can be found directly from the coordinates of its three projections. The momentum variables are chosen so that the spatial curves determined by the singular point and these variables have projection patterns which pass as close to the measured points as possible in all views in the sense of a least-squares fit. The orbits are helices modified by energy loss corrections. The details of this fitting program for both six and eight free parameters will appear in another journal.

All π^- events were first analyzed with an arbitrary incoming neutron direction using eight free parameters. The output of this program was used to determine the direction of the neutron beam $\hat{N}$ with respect to the bubble-chamber fiducial coordinate system. Using this value of $\hat{N}$, the events were then processed through a program in which there were six free momentum parameters. The output of both programs included the frame number of the event $\mathbf{r}_0$, the lengths of the three tracks, the value of the momenta, and a goodness-of-fit parameter χ^2.

On the basis of the χ^2 for an event and the lengths of the tracks involved a confidence level parameter was defined. All events for which this parameter had too low a value were remeasured and reprocessed. At the end of this initial measurement and the subsequent remeasurement 4079 of the 5208 events identified were accepted. In 92% of these events the results of the six parameter program were retained for comparison with theory. In the remaining 8% the answers given by the eight parameter program were used. For these 8% it was decided that the initiating neutron had scattered before undergoing reaction (2a). These events off secondary neutrons were signaled by having a poor χ^2 for the six parameter fit and a good χ^2 for the eight parameter fit. Also a large percentage of them had singular points outside the region of the main neutron beam.

Neutron Beam Spectrum

All recoil events found were measured and analyzed. The computer output included the recoil proton's momentum $\mathbf{P}_r$, the laboratory energy T of the incoming neutron, calculated on the assumption that its initial momentum $\mathbf{P}_n$ was parallel to $\hat{N}$, and a goodness-of-fit parameter χ^2. These events were divided into two classes, depending on whether their energy was greater or less than T_0, the threshold for π^- production. Those events for which $T<T_0$ were counted to see what fraction of the total number of recoil events were in this class, but were otherwise ignored.

All events for which $T>T_0$ were remeasured. A comparison of the results of the two measurements of each event determined the resolution function $R_M(T',T_i)$, defined so that $R_M(T',T_i)dT'$ is the probability that a track corresponding to an energy T_i is measured to have an energy within a range dT' of T'.

In addition to imprecise measurements, multiple Coulomb scattering also contributes to the energy resolution. In order to calculate this effect it was assumed that the hydrogen existed in the form of free atoms and that the Coulomb scattering could be treated in Born approximation. On this basis the effect of multiple Coulomb scattering was described in terms of a Gaussian resolution function $R_S(T_i,T)$, where $R_S(T_i,T)dT_i$ is the probability that an event of energy T leaves a track in the chamber corresponding to an energy within a range dT_i of T_i. The width of this Gaussian for the available track lengths was $14.3\ P_r/M$ MeV. This varied from 12.0 to 15.5 MeV over the energy range $T>T_0$. Both multiple-scattering and measurement errors can be combined to yield a total resolution function

$$R(T',T)=\int dT_i R_S(T_i,T)R_M(T',T_i).$$

The measured values of T were divided into 42 bins; the rth bin contained all events for which $T_r\leq T\leq T_{r+1}$. If the number of incoming neutrons within a range dT of energy T is $(dN/dT)dT$ and $\Delta N_R(r)$ is the number of events in the rth bin, then

$$\Delta N_R(r)=N_p\int_{T_r}^{T_{r+1}}dT'\int dTR(T',T)\frac{dN}{dT}\times\int d\omega\epsilon(\bar{\theta},T)\left(\frac{d\sigma}{d\omega}\right)_T. \quad (4)$$

$\epsilon(\bar{\theta},T)$ is the probability that a proton which recoils from an incoming neutron scattered through an angle $\bar{\theta}$ in the center of the mass will satisfy the visual criteria to be counted as a "recoil event." N_p is the number of target proton per (centimeter)^2 in the region $ACDE$ and $(d\sigma/d\omega)_T$ is the n-p differential cross section at laboratory energy T. $\epsilon(\bar{\theta},T)$ is a purely geometric factor which was calculated by Monte Carlo techniques. Define

$$g(T)=\int d\omega\epsilon(\bar{\theta},T)\left(\frac{d\sigma}{d\omega}\right)_T.$$

$g(T)$ can be calculated from the measured[6] values of $d\sigma/d\omega$ at $T=260$, 300, 380, 400, 580 MeV. Figure 6 shows a plot of $g(T)$ versus T. A broken line function is used to interpolate between the various measured points.

In order to calculate an analytic expression for (dN/dT), the spectrum was assumed to be of the

[6] W. M. Hess, Rev. Mod. Phys. **30**, 368 (1958).

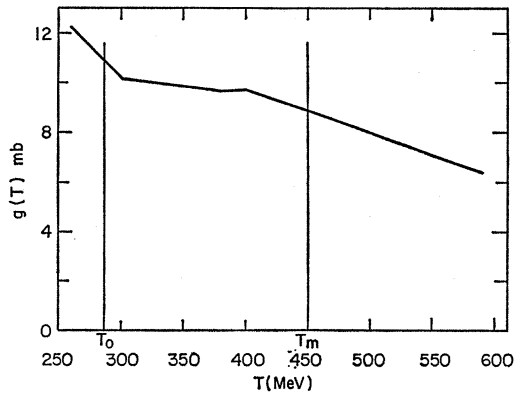

FIG. 6. Effective n-p cross section $g(T)$ versus T.

following form:

$T_0 \leq T \leq 310$ MeV;	(dN/dT) = constant = R
$310 \leq T \leq T_m$ = 442.5 MeV;	(dN/dT) = polynomial in T with 5 free parameters whose slope at 310 MeV = 0 and whose value at 310 MeV is R and at T_m is 0.0
$T \geq T_m$;	$(dN/dT) = 0.0$.

This form was fitted to $\Delta N_R(r)$ using least squares. Figure 7 show a plot of (dN/dT) versus T, subject to the normalization

$$\int \left(\frac{dN}{dT}\right) dT = 1 \quad \text{(for } T \text{ in units } m_\pi = 1\text{)}.$$

R was chosen so as to best fit the data from 220 to 310 MeV.

It will be noted that (dN/dT) as calculated possesses some rather extreme features such as a very sharp minimum at 324 and a shoulder at 350 MeV. These, very likely, are spurious effects caused by the fact that this spectrum is looked at with rather poor resolution. This experiment can hardly distinguish between a curve that wiggles many times within the resolution width and one that is flat. The resolution is also insufficient to see if the peak at 400 MeV might have some kind of fine structure, say, a flat top with sharp shoulders. Because of this the calculated curve for (dN/dT) can probably be in error by as much as ± 0.2 at any given energy.

Measurement of the recoil events not only yields information about the neutron energy spectrum, but also constitutes a measurement of $(d\sigma/d\omega)$ for a certain range of angles. From Eq. (4)

$$\frac{dN_R}{d(\cos\bar{\theta})} = 2\pi N_p \int dT \left(\frac{dN}{dT}\right) \epsilon(\bar{\theta},T) \left(\frac{d\sigma}{d\omega}\right)_T \qquad (5)$$

$dN_R/d(\cos\bar{\theta})$ is the density of events as a function of $\cos\bar{\theta}$. The function $\epsilon(\bar{\theta},T)(d\sigma/d\omega)_T$ can, to good approximation, be written in the form

$$\epsilon(\bar{\theta},T)(d\sigma/d\omega)_T = k(\bar{\theta})g(T)$$

in the energy range $T_0 \leq T \leq T_m$. With this approximation, Eq. (5) reduces to

$$dN_R/d(\cos\bar{\theta}) \sim k(\bar{\theta}).$$

Figure 8 shows a comparison of $k(\bar{\theta})$ determined from the data at 400 MeV with the histogram of $dN_R/d(\cos\bar{\theta})$. It is seen that these data are consistent with previous measurements of $d\sigma/d\omega$.

The average cross section for recoil events in the region $T \geq T_0$ is

$$\bar{\sigma}_R = \int_{T_0}^{T_m} dT \left(\frac{dN}{dT}\right) g(T) \Big/ \int_{T_0}^{T_m} dT \left(\frac{dN}{dT}\right) = 9.71 \text{ mb}.$$

This value will be used to place the π^- cross sections on an absolute basis.

COMPARISON OF THEORY AND EXPERIMENT

Form of the Distribution Function

The π^- events are described in terms of a distribution function $F(T,r,\mu_P,\mu_Q,\mu)$. μ_P, μ_Q, and μ are the cosines defined in the theoretical section; T is the incoming neutron laboratory energy; $r = Q/Q_m$, where Q_m is the maximum π^- momentum at energy T; and $Q = |\mathbf{Q}|$.

$$F dT d\mu_P d\mu_Q d\Phi$$

is the probability of a π^- event within ranges dT, dr, $d\mu_P$, $d\mu_Q$, and $d\Phi$ about T, r, μ_P, μ_Q, μ. Φ is the relative azimuth between $\mathbf{P}$ and $\mathbf{Q}$.

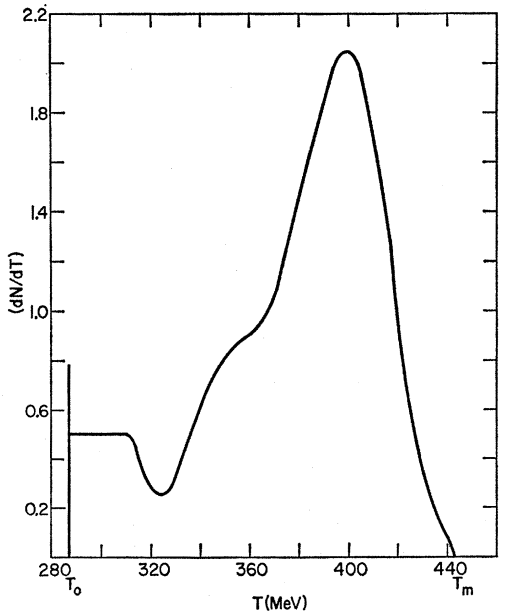

FIG. 7. Neutron differential energy spectrum dN/dT versus T used in analysis.

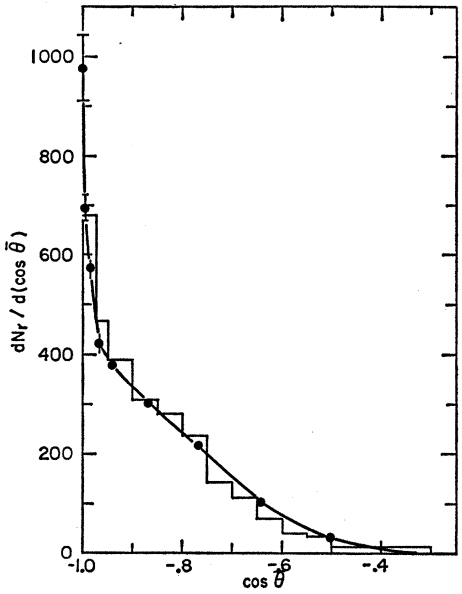

FIG. 8. Recoil proton angular spectrum $dN_R/d(\cos\theta)$ versus $\cos\bar{\theta}$.

$$d\Phi = d\mu/(1-\mu_P{}^2-\mu_Q{}^2-\mu^2+2\mu_P\mu_Q\mu)^{1/2}.$$

F is related to the transition probability f as follows:

$$FdTd\mu_P dr d\mu_Q d\Phi \sim \frac{1}{\beta_i}\left(\frac{dN}{dT}\right)dT\frac{f}{\Omega}[Q_m{}^3Pr^2(S-\Omega)dr] \times d\mu_P d\mu_Q d\Phi. \quad (6)$$

β_i is the relative velocity of the incoming nucleons in the center-of-mass system. S is the total center-of-mass energy and $\Omega=(1+Q^2)^{1/2}$ is the energy of the π^-. The factor $(1/\Omega)$ is the square of the normalization factor for the boson wave function. P and Q are related to S by the equation of energy conservation which can be written as

$$S=(1+Q^2)^{1/2}+(4M^2+P^2+Q^2)^{1/2} \quad (7)$$

to excellent approximation in the energy range $T_0 \leq T \leq T_m$ MeV.

It is convenient to define

$$dS=(2/\beta_i)(1/\Omega)[Q_m{}^3Pr^2(S-\Omega)dr]$$

and refer to it as an element of phase space (although properly only the term in square brackets comes from phase space) and to an integral of the form $\int\psi dS$ as an integral of ψ over phase space. Also let

$$d^5V = drdTd\mu_P d\mu_Q d\Phi$$

and

$$d^3\Theta = d\mu_P d\mu_Q d\Phi.$$

With these definitions, relation (6) reduces to

$$Fd^5V=(dN/dT)dTfdSd^3\Theta, \quad (8)$$

where the constant of proportionality has been absorbed in f. It is sometimes convenient to refer to the F distribution integrated over one or more of its independent variables. Such distributions will be denoted by writing F as a function of its remaining variables. For example, $F(r,T)=\int Fd^3\Theta$.

In the section on theory it was shown that the total transition probability can be written as the sum of partial probabilities

$$f=f_{Pp}+f_{Ps}+f_{Sp}+f_{Ss}+f_{PsPp}+f_{SpSs}, \quad (9a)$$

where each term is of the form

$$f_\lambda=G_\lambda(P,Q)H_\lambda(\mu_P,\mu_Q,\mu). \quad (9b)$$

The G's are functions of the momentum variables only, the H's are polynomials in the angle variables, and λ can stand for any of the subscripts appearing in (9a). It is convenient to define the integrals

$$\Lambda_\lambda=\int\frac{dN}{dT}dTG_\lambda(P,Q)dS,$$

and rewrite Eqs. (3a) to (3f) as follows:

$$f_{Pp}=(P^2Q^2/\Lambda_{Pp})[a_{Pp}+\alpha_2'(3\mu_P{}^2-1)+\alpha_3'(3\mu_Q{}^2-1)+\alpha_4'(3\mu^2-1)+\alpha_5'(9\mu_P\mu_Q\mu-1)], \quad (10a)$$

$$f_{Ps}=(P^2/\Lambda_{Ps})[a_{Ps}+\beta_2'(3\mu_P{}^2-1)], \quad (10b)$$

$$f_{Sp}=(h^2Q^2/\Lambda_{Sp})[a_{Sp}+\gamma_2'(3\mu_Q{}^2-1)], \quad (10c)$$

$$f_{Ss}=(h^2/\Lambda_{Ss})a_{Ss}, \quad (10d)$$

$$f_{PsPp}=(P^2Q/\Lambda_{PsPp})[2c_1'\mu_Q+6c_2'\mu_P\mu_Q+6c_3'\mu_P\mu], \quad (10e)$$

$$f_{SpSs}=(h^2Q/\Lambda_{SpSs})[2d_1'\mu_Q]. \quad (10f)$$

The constants that appear in (10a) to (10f) are related to those in (3a) through (3f) by

$$\alpha_1=\frac{a_{Pp}-\alpha_2'-\alpha_3'-\alpha_4'-\alpha_5'}{\Lambda_{Pp}};\quad \alpha_2=\frac{3\alpha_2'}{\Lambda_{Pp}};\quad \alpha_3=\frac{3\alpha_3'}{\Lambda_{Pp}};$$

$$\alpha_4=\frac{3\alpha_4'}{\Lambda_{Pp}};\quad \alpha_5=\frac{9\alpha_5'}{\Lambda_{Pp}};$$

$$\beta_1=(a_{Ps}-\beta_2')/\Lambda_{Ps};\quad \beta_2=3\beta_2'/\Lambda_{Ps};$$

$$\gamma_1=(a_{Sp}-\gamma_2')/\Lambda_{Sp};\quad \gamma_2=3\gamma_2'/\Lambda_{Sp};$$

$$\delta_1=(a_{Ss}/\Lambda_{Ss});$$

$$c_1=2c_1'/\Lambda_{PsPp};\quad c_2=6c_2'/\Lambda_{PsPp};\quad c_3=6c_3'/\Lambda_{PsPp};$$

$$d_1=(2d_1'/\Lambda_{SpSs}).$$

With these definitions the following normalization conditions hold for all λ:

$$\int\left(\frac{dN}{dT}\right)dTG_\lambda dS=1 \quad (11a)$$

$$\int d^3\Theta H_\lambda=8\pi a_\lambda \quad (\text{note: } a_{PsPp}=a_{SpSs}=0). \quad (11b)$$

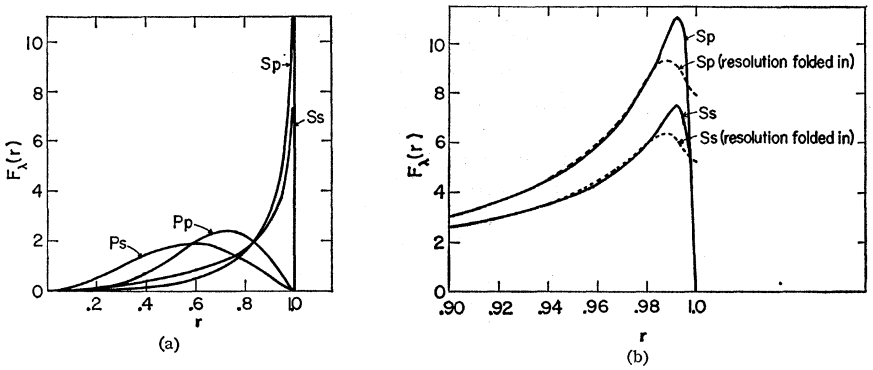

FIG. 9. (a) Theoretical forms of the *Ss*, *Pp*, *Ps*, *Ps* distribution versus r. (b) Same as Fig. 10(a) for *Sp* and *Ss* in the region $0.9<r$. Also shown are the modifications due to resolution.

The distribution F can be expected to describe the density of events only if the tracks are measured with perfect accuracy. In order to estimate the resolution with which the various parameters describing an event are measured, 700 events distributed uniformly through the whole sample were remeasured and the old and new results compared. If the resolution function for parameter ν is assumed to have the form

$$R(\nu,\nu')=\frac{1}{(2\pi)^{1/2}\sigma}e^{-(\nu-\nu')^2/2\sigma^2},$$

the following widths were obtained:

Parameter	σ
T	3 MeV
r	0.007
μ_P	0.01
μ_Q	0.008
μ	0.01

As with recoil events, multiple scattering also limits the accuracy of the parameters determined by measuring a π^- event. The size of this effect was calculated to correspond to a Gaussian resolution function of widths:

Parameter	σ
T	6.5 MeV
r	0.011
μ_P	0.013
μ_Q	0.010
μ	0.014

It is seen from the form of F as a function of the angle variables, namely low-order polynomials in the various μ's, that all peaks and valleys in their distribution will occur over ranges of these parameters very large compared to the corresponding σ's, so that the effect of finite resolution can be neglected. The same is not true for the variables T and r. To illustrate how resolution modifies the distribution of these parameters, consider Eq. (6) integrated over Θ and T with (9a) and (9b) substituted for f. It is seen that the distribution of r is of the form

$$F(r)=\frac{1}{8\pi}\int d^3\Theta dTF=\sum_\lambda \int dT\left(\frac{dN}{dT}\right)a_\lambda G_\lambda\frac{dS}{dr}$$
$$=\sum_\lambda a_\lambda F_\lambda(r).$$

Figure 9(a) is a graph of $F_\lambda(r)$ versus r for the *Ps*, *Pp*, *Sp*, and *Ss* transitions. The *Sp* and *Ss* distributions show very sharp peaks near $r=0.99$. The finite resolution rounds these peaks as shown on an expanded scale in Fig. 9(b). The peaks in the distribution $F(T)$ are also rounded off. In comparing the theoretical distribution with the experimental data, the resolution in "r" and "T" was folded into F.

To see if all the f_λ are actually present in F, $F(r,T)$ was fitted to the experimental results by means of a maximum likelihood calculation

$$F(r,T)drdT=\left(\frac{dN}{dT}\right)dTdS\left[a_{Pp}\frac{P^2Q^2}{\Lambda_{Pp}}+a_{Ps}\frac{P^2}{\Lambda_{Ps}}+a_{Sp}\frac{h^2Q^2}{\Lambda_{Sp}}+a_{Ss}\frac{h^2}{\Lambda_{Ss}}\right]. \quad (12)$$

If the normalization condition

$$\int F(r,T)drdT=1$$

is imposed, it follows from (11a) that

$$a_{Pp}+a_{Ps}+a_{Sp}+a_{Ss}=1. \quad (13)$$

Equation (13) was imposed as a constraint on the parameters in the likelihood calculation. a_{Ps} at maximum likelihood had the value 0.002 with a standard deviation of 0.018, a value clearly consistent with 0. This says that the intensity of the *Ps* transitions is far too small to be detected by this experiment. Thus, a_{Ps} and β_2 were set equal to zero and the number of free parameters associated with the final state was reduced by 2. Note that if the *Ps* amplitudes were rigorously

zero then the $PsPp$ interference terms $(c_1; c_2; c_3)$ would also necessarily be zero, but it is well known that weak transitions can lead to appreciable interference terms so that it was not felt that c_1, c_2, and c_3 could be safely ignored.

With the elimination of the Ps terms there remain 12 parameters to describe the final state, subject to normalization condition (13) with $a_{Ps}=0$. These parameters and the associated error matrix were found by comparing the theoretical form of the final state, Eqs. (10a) through (10f), with the experimental data by means of a maximum likelihood calculation. The result of this search in parameter space is as follows:

$$\begin{aligned}
f_{Pp}&=P^2Q^2[(1.32\pm0.13)+(0.92\pm0.21)\mu_P{}^2\\
&\quad+(-0.05\pm0.21)\mu_Q{}^2+(-0.13\pm0.19)\mu^2\\
&\quad+(0.76\pm0.48)\mu\mu_P\mu_Q],\\
f_{Sp}&=h^2Q^2[(-0.11\pm0.045)+(1.32\pm0.08)\mu_Q{}^2],\\
f_{Ss}&=h^2[(0.25\pm0.03)],\\
f_{PsPp}&=P^2Q[(0.17\pm0.06)\mu_Q+(0.37\pm0.16)\mu_P{}^2\mu_Q\\
&\quad+(-0.22\pm0.10)\mu\mu_P],\\
f_{SpSs}&=h^2Q[(0.73\pm0.04)\mu_Q],
\end{aligned}\tag{14a}$$

$$\begin{aligned}
F(r,T,\mu_P,\mu_Q,\mu)d^5V&\\
=(1/8\pi\Lambda_{Ss})(dN/dT)dT\,fdSd^3\Theta,&\\
\Lambda_{Ss}=35.25.&
\end{aligned}\tag{14b}$$

The listed uncertainties were calculated by standard procedures from the error matrix.

With this definition of F and f, it follows that

$$\int_{T_0}^{T_m}dT\int F(r,T,\mu_P,\mu_Q,\mu)drd^3\Theta=1.\tag{14c}$$

In all the above equations it is assumed all momentum variables and masses are expressed in units where $m_\pi=1$.

F_λ is related to the differential π^- production cross section in the λth channel $d\sigma_\lambda(r,T,\mu_P,\mu_Q,\mu)$ as follows:

$$\left(\frac{dN}{dT}\right)dTd\sigma_\lambda(r,T,\mu_P,\mu_Q,\mu)=\bar{\sigma}F_\lambda d^5V\int_{T_0}^{T_m}dT\left(\frac{dN}{dT}\right),\tag{15}$$

where

$$\bar{\sigma}=\int_{T_0}^{T_m}dT\left(\frac{dN}{dT}\right)\sigma_T(T)\Big/\int_{T_0}^{T_m}dT\left(\frac{dN}{dT}\right).$$

σ_T is the total π^- production cross section at energy T.

The value of $\bar{\sigma}$ can be found directly by comparing the number of π^- events with $T<T_m$ per gram track length in H_2 with the number of recoil events for the same track length and in the same energy range. The value of $\bar{\sigma}$ is

$$\bar{\sigma}=53.3\pm4.8\ \mu\text{b}.$$

One-Dimensional Distributions

Figure 10(a) is a graph of $N(T)$ $[N(\nu)=4079F(\nu)]$ found from the likelihood fit (smooth curve) and the experimental distribution (the histogram). While the two curves do not agree within statistics, it was felt that this disagreement was a reflection of the rather poor determination of (dN/dT), rather than an indication that the theory is incorrect. If (dN/dT) (Fig. 7) was 10% lower at its peak, with a corresponding increase in width, the two curves of Fig. 10(a) would be compatible. Such an overestimate is quite possible in view of the limited resolution in the neutron spectrum measurement.

Figure 10(b) is the corresponding graph for $N(r)$. Here the agreement between theory and experiment is within statistics, except for the region $r>0.9$, which will be considered in more detail later. This agreement represents a fairly good check on the theory, since only two parameters could be varied to optimize the fit, namely, a_{Pp} and a_{Sp} ($a_{Ps}=0$ and $a_{Ss}=1-a_{Pp}-a_{Sp}$). Writing Eq. (12) with $a_{Ps}=0$

$$\begin{aligned}
F(r,T)drdT=\left(\frac{dN}{dT}\right)dTdS\Bigg[&\frac{h^2}{\Lambda_{Ss}}+a_{Pp}\left(\frac{P^2Q^2}{\Lambda_{Pp}}-\frac{h^2}{\Lambda_{Ss}}\right)\\
&+a_{Sp}\left(\frac{h^2Q^2}{\Lambda_{Sp}}-\frac{h^2}{\Lambda_{Ss}}\right)\Bigg].
\end{aligned}$$

It is interesting to look at the above equation, integrated over T at $r=0.85$.

$$F(r=0.85)dr=(1.96-0.125a_{Pp}+0.115a_{Sp})dr.$$

Since both a_{Pp} and a_{Sp} must be greater than 0 and less than 1 [see (13)], $F(r=0.85)$ must lie between 1.83 and 2.07. In other words, the value of $F(r)$ at $r=0.85$ is 1.95 (1 ± 0.06), if this theory is valid, independent of any parameter. In this region, the experimental data does agree with the theory to $1\frac{1}{2}$ standard deviations.

Figures 10(c), 10(d), and 10(e) show both the theoretical and experimental distributions of the angle variables. The theoretical distributions are

$$\begin{aligned}
F(\mu_P)&=1+(0.138\pm0.016)(3\mu_P{}^2-1),\\
F(\mu_Q)&=1+(0.649\pm0.027)\mu_Q\\
&\quad+(0.245\pm0.017)(3\mu_Q{}^2-1),\\
F(\mu)&=1+(0.014\pm0.016)(3\mu^2-1).
\end{aligned}$$

They are in good agreement with the experimental results. In particular there is no evidence that higher powers of the various cosines are needed in F.

It is interesting to display the directional correlation of the two outgoing protons. Since the protons are much more massive than the π^-, those configurations where they are nearly parallel correspond to the π^- having at least 85% of the available kinetic energy. Such unbalanced distributions are suppressed by phase

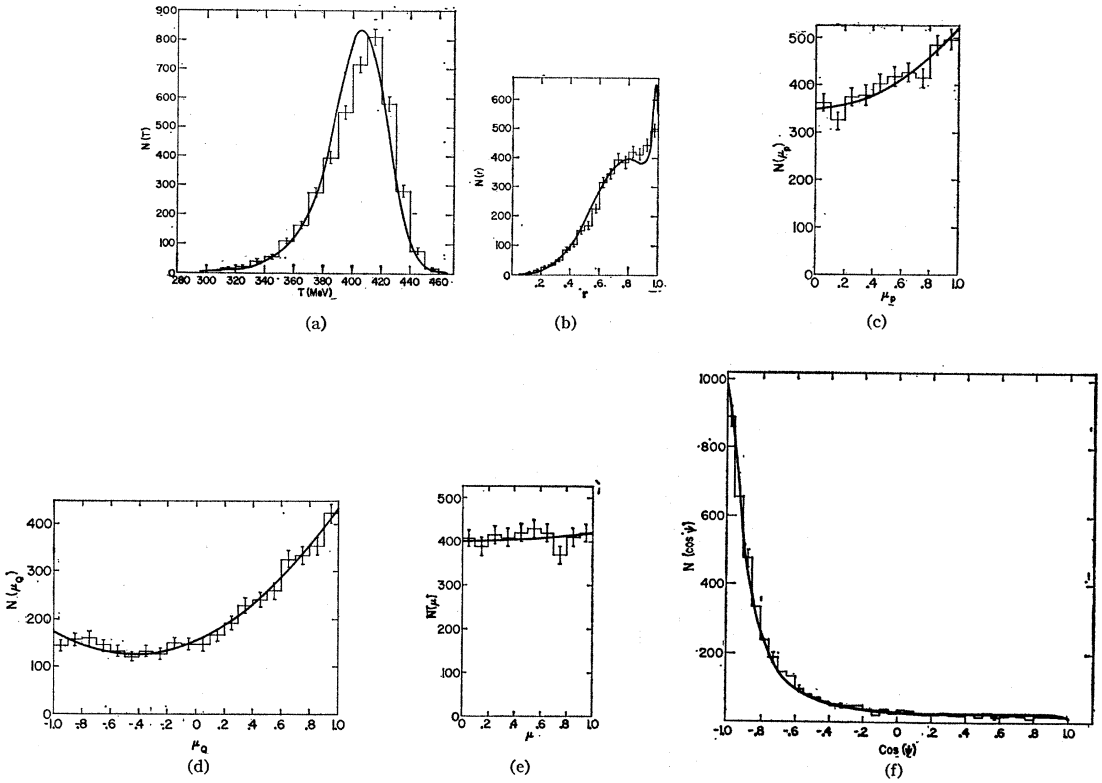

FIG. 10. One-dimension distributions $N(\nu)$ versus ν for $\nu=T$, r, μ_P, μ_Q, μ, and ψ. The maximum-likelihood results are shown along with the experimental results.

space. The only configuration at all close to equipartition corresponds to $\cos(\psi)$ close to -1, where ψ is the angle between the two protons. This effect is shown in Fig. 10(f), where the distribution of $\cos(\psi)$ has been plotted.

Figure 11 shows the distribution $N(r)$ for $r>0.9$ and a histogram of the experimental data in this region. It seems clear that there is a systematic departure of the theoretical curve from the experimental results. This disagreement may have a physical explanation as follows: The sharp peak at high r in the Ss and Sp distributions is due to the attractive $^1S_0$ interaction of the two final-state protons. In calculating the effect of this interaction the presence of the π^-, which also interacts strongly with the two nucleons, is ignored.

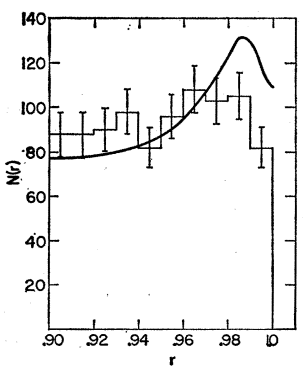

FIG. 11. $N(r)$ versus r for $r>0.9$.

The π^--proton interaction may spread out the Ss and Sp distributions at large r enough to account for the lack of a peak in the experimental data at $r=0.985$.

Transition Amplitudes

In general, there are not nearly enough constants defined in the transition probability f to determine the amplitudes of the various transitions listed in Table I. If certain assumptions are made, which will be detailed later, the value of some can be found. In other cases it is instructive to display a set of amplitudes which lead to the correct terms in f just to show that the distribution found by the maximum likelihood search is consistent with the theory of Gell-Mann and Watson.[4] In no case is the assertion made that the amplitudes to be listed are uniquely determined. Normalization is chosen so that if a is the amplitude of a transition from an incoming $^{2S+1}L_j$ state then the intensity of this transition, taken from the numbers given in Eq. (14a), is $[(2j+1)/(2L+1)]|a|^2$.

The situation, with regard to finding amplitudes is particularly hopeless in the transitions to final Ps states. There are a large number of such transitions (three $I=0$ and two $I=1$) and the only information in f about them are the values of the three $PsPp$ interference terms. The only use that will be made of these interference terms is to set a lower limit on the amount of Ps state that is present. Otherwise they will be

treated as having strictly zero amplitudes and all Ps and $PsP\phi$ interference terms will be ignored.

The transitions can be divided into four sets. No interference occurs between members of different sets.

(a) singlet $\rightarrow$ singlet,

(b) triplet $\rightarrow$ singlet,

(c) singlet $\rightarrow$ triplet,

(d) triplet $\rightarrow$ triplet.

Since there are no interference terms linking the above sets, it is clear that each can be assigned an arbitrary over-all phase with respect to the others.

(a) Incoming singlet to outgoing singlet. There are no allowed transitions of this type in Table I.

(b) Incoming triplet to outgoing singlet. This includes the transitions

$$I=1,\quad {}^3P_0\rightarrow {}^1S_0s_0,\quad \text{amplitude } ah;$$
$$I=0,\begin{cases}{}^3S_1\rightarrow {}^1S_0p_1, & \text{amplitude } b_1{}^0hQ;\\ {}^3D_1\rightarrow {}^1S_0p_1, & \text{amplitude } b_2{}^0hQ.\end{cases}$$

These states lead to a transition probability of the form

$$h^2(\tfrac{1}{3}|a|^2+2Q\ \mathrm{Re}\{a^*[b_1{}^0-2(1/10)^{1/2}b_2{}^0]\}\mu_Q +3Q^2\{|b_1{}^0+(1/10)^{1/2}b_2{}^0|^2 +[|b_1{}^0-2(1/10)^{1/2}b_2{}^0|^2 -|b_1{}^0+(1/10)^{1/2}b_2{}^0|^2]\mu_Q{}^2\}).$$

Comparing this with the relevant terms in (14a) it is seen that

$$a^2=0.76, \tag{16a}$$
$$2\ \mathrm{Re}\{a^*[b_1{}^0-2(1/10)^{1/2}b_2{}^0]\}=0.73, \tag{16b}$$
$$3|b_1{}^0+(1/10)^{1/2}b_2{}^0|^2=-0.11, \tag{16c}$$
$$3[|b_1{}^0-2(1/10)^{1/2}b_2{}^0|^2 -|b_1{}^0+(1/10)^{1/2}b_2{}^0|^2]=1.32. \tag{16d}$$

It is clear that (16c) cannot be satisfied. This is because the distribution f_{Sp}, which can be written

$$f_{Sp}=h^2Q^2[0.33+0.44(3\mu_Q{}^2-1)]$$

is not positive definite. A possible explanation for this is that there is a small amount of the transition

$$I=1,\quad {}^3P_2\rightarrow {}^1S_0d_2,\quad \text{amplitude } \sim h^2Q^2. \tag{17}$$

The interference between (17) and the ${}^3P_0\rightarrow {}^1S_0s_0$ transitions would be proportional to $h^2Q^2(3\mu_Q{}^2-1)$ and would be counted as part of f_{Sp}. If the size of this interference term is 0.11 $h^2Q^2(3\mu_Q{}^2-1)$, just enough to make the pure Sp contribution positive definite, then only enough of transition (17) to account for 1% of the production events need be postulated. If this interference term is subtracted from f_{Sp} then Eqs. (16) will now read

$$3|b_1{}^0+(1/10)^{1/2}b_2{}^0|^2=0, \tag{16c}'$$
$$3|b_1{}^0-2(1/10)^{1/2}b_2{}^0|=1.00. \tag{16d}'$$

If a is chosen real and positive to fix the arbitrary phase, the set of Eqs. (16a), (16b), (16c), (16d) have the solutions

$$a=0.87,$$
$$b_1{}^0=0.19e^{\pm i\phi},$$
$$b_2{}^0=(10)^{1/2}b_1{}^0,$$

where $\phi=0.75$ rad.

(c) Incoming singlet to outgoing triplet. This set includes the transitions

$$I=0:\quad {}^1P_1\rightarrow {}^3P_0p_1,\quad \text{amplitude } d_0{}^0PQ,$$
$${}^1P_1\rightarrow {}^3P_1p_1,\quad \text{amplitude } d_1{}^0PQ,$$
$${}^1P_1\rightarrow {}^3P_2p_1,\quad \text{amplitude } d_2{}^0PQ.$$

There are also $I=0$ transitions leading to Ps final states which, as mentioned before, will be ignored.

Defining

$$\lambda'=-\tfrac{3}{2}(1/15)^{1/2}d_2{}^0-\tfrac{1}{2}d_1{}^0,$$
$$\nu'=(1/15)^{1/2}d_2{}^0-(\tfrac{1}{3})^{1/2}d_0{}^0,$$
$$\sigma'=-\tfrac{3}{2}(1/15)^{1/2}d_2{}^0+\tfrac{1}{2}d_1{}^0,$$

the f_{Pp} resulting from the above transitions is of the form

$$9P^2Q^2[|\lambda'|^2\mu_P{}^2+|\nu'|^2\mu_Q{}^2+|\sigma'|^2\mu^2 +2\ \mathrm{Re}[\lambda'\sigma'^*+\nu'\sigma'^*+\lambda'\nu'^*]\mu_P\mu_Q\mu]. \tag{18}$$

The experimental value of f_{Pp} is

$$f_{Pp}=P^2Q^2[1.32+0.92\mu_P{}^2-0.05\mu_Q{}^2 -0.13\mu^2+0.76\mu_P\mu_Q\mu].$$

This implies that all of the $P\phi$ intensity cannot be from $I=0$ transitions.

(d) Incoming triplet to outgoing triplet. This set includes the transitions

$$I=1:\quad {}^3P_0\rightarrow {}^3P_1p_0,\quad \text{amplitude } d_{10}PQ,$$
$${}^3P_1\rightarrow {}^3P_0p_1,\quad \text{amplitude } d_{01}PQ,$$
$${}^3P_1\rightarrow {}^3P_1p_1,\quad \text{amplitude } d_{11}PQ,$$
$${}^3P_1\rightarrow {}^3P_2p_1,\quad \text{amplitude } d_{21}PQ,$$
$${}^3P_2\rightarrow {}^3P_1p_2,\quad \text{amplitude } d_{12}PQ,$$
$${}^3P_2\rightarrow {}^3P_2p_2,\quad \text{amplitude } d_{22}PQ.$$

The $I=0$ transitions leading to Ps final states will not be considered.

Defining

$$\alpha=(\tfrac{1}{3})^{1/2}d_{01}-\tfrac{1}{2}d_{11}+\tfrac{1}{2}(1/15)^{1/2}d_{21}-\tfrac{1}{2}d_{12}-\tfrac{1}{2}(\tfrac{1}{3})^{1/2}d_{22},$$
$$\beta=\tfrac{1}{2}d_{11}-\tfrac{3}{2}(1/15)^{1/2}d_{21}-\tfrac{1}{2}d_{12}+\tfrac{1}{2}(\tfrac{1}{3})^{1/2}d_{22},$$
$$\gamma=3(1/15)^{1/2}d_{21}+(\tfrac{1}{3})^{1/2}d_{22},$$
$$\delta=-\tfrac{1}{2}d_{11}-\tfrac{3}{2}(1/15)^{1/2}d_{21}+\tfrac{1}{2}d_{12}+\tfrac{1}{2}(\tfrac{1}{3})^{1/2}d_{22},$$
$$\epsilon=-(\tfrac{1}{3})^{1/2}d_{01}+(1/15)^{1/2}d_{21}-(\tfrac{1}{3})^{1/2}d_{22},$$
$$\rho=\tfrac{1}{3}d_{10}-\tfrac{1}{3}d_{12}+(\tfrac{1}{3})^{1/2}d_{22},$$
$$\nu=-\tfrac{1}{3}d_{10}-\tfrac{2}{3}d_{12},$$
$$\lambda=(\tfrac{1}{3})^{1/2}d_{01}+\tfrac{1}{2}d_{11}+\tfrac{1}{2}(1/15)^{1/2}d_{21}+\tfrac{1}{2}d_{12}-\tfrac{1}{2}(\tfrac{1}{3})^{1/2}d_{22},$$
$$\sigma=-\tfrac{1}{3}d_{10}+\tfrac{1}{3}d_{12}+(\tfrac{1}{3})^{1/2}d_{22},$$

and

$$q_1=|\alpha-\gamma|^2+|\lambda|^2+2|\sigma|^2,$$
$$q_2=|\epsilon|^2+|\rho|^2,$$
$$q_3=|\delta|^2+|\nu|^2,$$
$$q_4=|\alpha+\gamma|^2+|\lambda|^2,$$
$$q_5=|\beta|^2,$$

the distribution resulting from the above transitions is of the form

$$(9/4)P^2Q^2[q_1+(2q_2-q_1)\mu_Q{}^2+(2q_3-q_1)\mu_P{}^2+(q_4-q_1)\mu^2+(2q_1-2q_2-2q_3+4q_5)\mu_P\mu_Q\mu]. \quad (19)$$

If the assumption is made the $d_0{}^0=d_1{}^0=d_2{}^0=0$, i.e., the (c) set is absent, then the appropriate values of the q's to produce the Pp terms in (14a) are

$$q_1=0.59,$$
$$q_2=0.50,$$
$$q_3=0.28,$$
$$q_4=0.53,$$
$$q_5=0.315.$$

Note that under the above assumption the values of all the q's are positive, in agreement with the positive definite expressions listed for the q's.

To demonstrate that the experimental f_{Pp} is consistent with all the Pp terms being due to $I=1$ transitions it is only necessary to show that there exists a set of amplitudes which will produce the coefficients in f_{Pp}. One such set is

$$d_{10}=0.19,$$
$$d_{01}=-0.35,$$
$$d_{11}=0,$$
$$d_{21}=1.16,$$
$$d_{12}=0.04,$$
$$d_{22}=-0.33.$$

There are many other such sets.

One can use the fact that the form (18) for the $I=0$ transitions to final Pp states cannot by itself fit the experimental data to put an upper limit on the amount of the Pp final state which can be due to these $I=0$ transitions. The amount of $I=1$ Pp final state is found by integrating (19) over Θ.

$$\text{Intensity}=(\tfrac{1}{2}q_1+q_2+q_3+\tfrac{1}{2}q_4+q_5)P^2Q^2.$$

Changing the values of $d_0{}^0$, $d_1{}^0$, and $d_2{}^0$ from 0 cannot change the value of q_1 since (18) has no constant term. Also since q_2, q_3, q_4, and q_5 are positive definite they cannot be less than 0. This implies that the amount of $I=1$ transition to a final Pp state is $\geq\frac{1}{2}q_1=0.29=18\%$ of the total Pp intensity [see (18)]. Thus the amount of $I=0$ Pp intensity is $\leq(82\pm2)\%$ of total Pp intensity. That this upper limit can be reached is demonstrated by the fact that the amplitude set,

$$I=0:\quad d_0{}^0=-0.075+0.31i,\quad d_1{}^0=0.135,\quad d_2{}^0=1.12,$$
$$I=1:\quad d_{10}=-0.31,\quad d_{01}=-0.18,\quad d_{11}=0.16,$$
$$d_{21}=0.20,\quad d_{12}=0.16,\quad d_{22}=0.27,$$

will produce the observed Pp distribution and has 82% of the intensity in the $I=0$ transitions.

The value of the $PpPs$ interference terms in Eq. (14a) can be used to put a lower limit on the amount of Ps transition in the sample. The result of this calculation is that the intensity of the Ps transitions is greater than or equal to $(0.01\pm0.004)P^2$. This says that at least 1% of the events belonged to a Ps final state.

COMPARISON WITH OTHER EXPERIMENTS

If Eq. (15) is integrated over all variables but T and divided by dN/dT, then

$$\sigma_\lambda(T)=\bar{\sigma}a_\lambda F_\lambda(T)\int_{T_0}^{T_m}\left(\frac{dN}{dT}\right)dT\Big/\left(\frac{dN}{dT}\right),$$

where $\sigma_\lambda(T)$ is the total cross section in channel λ at energy T. Figure 12 contains a graph of σ_{Ss} (curve I), $\sigma_{Ss}+\sigma_{Pp}$ (curve III), and $\sigma_T=\sigma_{Ss}+\sigma_{Sp}+\sigma_{Pp}$ (curve IV).

σ_T can be expressed in terms of the cross section for transitions between states of definite nucleon-nucleon isotopic spin as,

$$\sigma_T=\tfrac{1}{2}\sigma_{01}+\tfrac{1}{2}\sigma_{11}.$$

On the basis of this experiment alone, it is not possible to find σ_{01} and σ_{11} separately, inasmuch as the states belonging to the Pp channel can result from either 01 or 11 transitions. In the last section it was shown that at least 18% of the total Pp cross section must be due to 11 transitions, so that $\sigma_{Ss}+0.18\sigma_{Pp}$ (curve II, Fig. 12) is a lower limit to $\frac{1}{2}\sigma_{11}$. Moreover, since Sp final states can only result from 01 transitions, a lower limit of σ_{sp} can be placed on the value of $\frac{1}{2}\sigma_{01}$. These results are summarized in the inequality

$$\sigma_{Ss}+0.18\sigma_{Pp}\leq\tfrac{1}{2}\sigma_{11}\leq\sigma_{Ss}+\sigma_{Pp}.$$

Graphically this means that a plot of $\frac{1}{2}\sigma_{11}$ should lie somewhere between curves II and III.

Dunaitsev and Prokoskin[3d] have measured the cross section of

$$p+p\rightarrow\pi^0+p+p$$

which is pure σ_{11}, in the region from threshold to 635 MeV. Their measured points and experimental errors in the energy region $T_0<T<445$ MeV are shown by circles with error flags in Fig. 12. Curve B (dashed line) is the curve they drew through these points as the best fit to their data. It does indeed lie between curves II and III except at very low energy. Also shown is curve

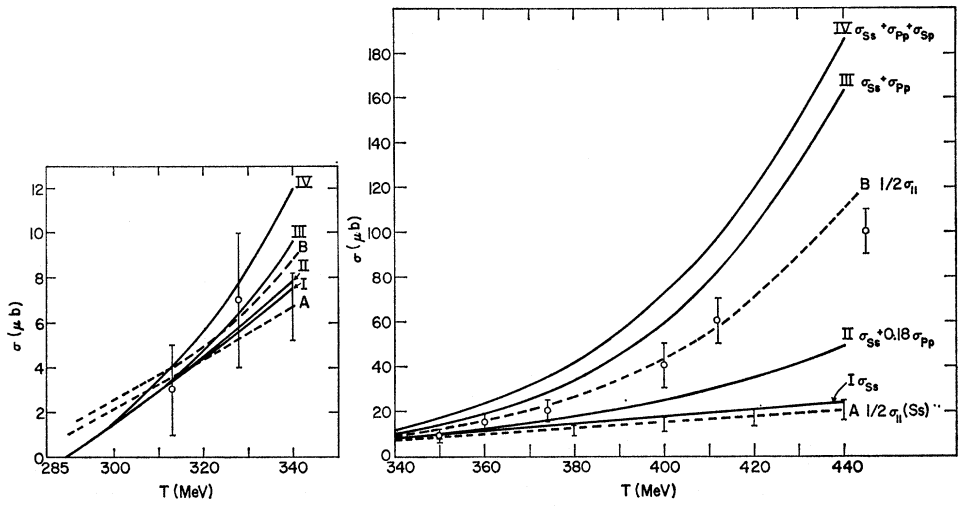

FIG. 12. Total cross sections versus T.

A (dashed line) which is their estimate of the contribution of σ_{Ss} to σ_{11}. It is in rather good agreement with curve I which is σ_{Ss} as found in this experiment.

According to the combined π^0 and π^- data it appears that the most likely division of the Pp intensity is about 40% $I=0$ and 60% $I=1$. That the nonresonant $I=0$ Pp transition should be comparable to the $I=1$ Pp transitions, the type favored by the 3-3 resonance, is inconsistent with Mandelstam's resonance theory even when modified to include nonresonant states favored by the final-state nucleon-nucleon interaction. This casts doubt on the theory's validity in this low-energy region. This conclusion, however, is based on the comparison of absolute cross sections from two different experiments, and is probably subject to large experimental error.

The value of σ_T at 409 MeV found from this experiment is 90 ± 8 μb, whereas the value found by Yodh[7] at this energy is quoted as $160+40$ μb. Yodh's angular distribution, at 409 MeV (for π^- production) is

$$(1.07\pm0.39)+(1.38\pm0.78)\mu_Q+(0.57\pm1.40)\mu_Q^2.$$

In this experiment the best value for this distribution with the same normalization is

$$(0.97\pm0.03)+(0.73\pm0.05)\mu_Q+(0.88\pm0.09)\mu_Q^2$$

in substantial agreement with Yodh's result.

The value found by Pondrom[8] for the Ps contribution to σ_{11} in the reaction $p+p\rightarrow\pi^++p+n$ at 450 MeV would indicate that

$$\int d\Theta f_{Ps}\geqslant(0.78\pm0.19)P^2.$$

This is altogether inconsistent with the value of the Ps intensity indicated by this experiment, which is on the order of $0.015P^2$ for both $I=0$ and $I=1$ transitions. This reinforces Pondrom's speculation that he was really seeing a transition to a final Ds state belonging to σ_{10}.

CONCLUSION

The phenomenological, near-threshold theory of Gell-Mann and Watson has been subjected to a detailed test by this experiment. In general, the agreement with the experimental data is excellent. There is some indication that there exists an interference term between two $I=1$ transitions ${}^3P_0\rightarrow{}^1S_0s_0$ and ${}^3P_2\rightarrow{}^1S_0d_2$, but this is the only manifestation of any orbital angular momentum states higher than $l=1$. Also there exists some discrepancy in the distribution of r for high r. This may be due to neglecting the effect of the π^- in calculating the modification of the transition probability introduced by the final-state ${}^1S_0$ p-p interaction.

ACKNOWLEDGMENTS

The author wishes to express his appreciation to Professor S. C. Wright who suggested this problem and helped in the preparation, execution, and analysis of the experiment. In particular, I wish to thank him for his help in "debugging" the many computer programs which were necessary to arrive at meaningful data from the initial set of photographs. The experiment was executed with a bubble chamber designed by Professor R. H. Hildebrand. P. K. Kloeppel and H. Kobrak spent many months with me in the design of its associated electrons. R. H. Hildebrand, M. Pyka, T. Denton, and S. Lucero kept the chamber in stable operating condition throughout the exposure of the film. S. Cheung

[7] G. Yodh, Phys. Rev. **98**, 1330 (1955).
[8] L. G. Pondrom, Phys. Rev. **114**, 1623 (1959).

and V. Zavitkowsky performed most of the tedious task of locating the events, and their many months of scanning were characterized by uniformly high accuracy. L. Seefeldt assisted in the design and built the measuring tables, and kept them in excellent operating condition. To all those mentioned above, and to many others, without whose help this experiment would have been impossible, go my sincere thanks.

PHYSICAL REVIEW VOLUME 138, NUMBER 5B 7 JUNE 1965

Dynamical Model of the Σ†

BORIS KAYSER*
California Institute of Technology, Pasadena, California
(Received 4 September 1964; revised manuscript received 11 January 1965)

In the spirit of the bootstrap hypothesis, a dynamical model is developed for the Σ hyperon, taking into account the $\pi\Lambda$ and $\pi\Sigma$ channels. Born amplitudes for the exchange of Λ, Σ, Y_1^* (1385 MeV), Y_0^* (1405 MeV), and ρ form the inputs to dynamical calculations that are based on the matrix ND^{-1} method and are intended partly as a practical study of this technique. It is shown that the ND^{-1} formalism can be trivially extended to handle the situation where an input force cut overlaps the unitarity cut below physical threshold.

In the dynamical calculations, the properties of all particles other than the Σ are taken from experiment, or, where they are experimentally uncertain, estimated on the basis of current theoretical ideas and then varied. The cutoff which governs the damping of the input amplitudes at high energies is also varied. It is found that quite a few combinations of the experimental unknowns and the cutoff do lead to a self-consistent $\frac{1}{2}^+$, $I=1$, $\pi\Lambda$-$\pi\Sigma$ bound state, identified as the Σ, with reasonable values for the mass M_Σ and couplings $g_{\pi\Lambda\Sigma}^2/4\pi$ and $g_{\pi\Sigma\Sigma}^2/4\pi$. These results favor the conjecture that the Σ is a composite particle.

I. INTRODUCTION

THE bootstrap idea is that the family of strongly interacting particles generates itself. Each particle is a composite object, being a bound or resonant state of all the multiparticle systems with which the various conservation laws allow it to communicate. The binding forces come from exchange of the strongly interacting particles themselves; hence the self-generation.

In practice, a realistic calculation which simultaneously bootstraps all of the baryons and mesons would be out of the question. The bootstrap hypothesis can be tested, however, by selecting some specific particle (A), and inquiring whether the strongly interacting family generates *it*. In other words, we assume that all the particles other than A already exist with their observed properties, and try to see whether, in such a universe, a particle with the quantum numbers of A should also exist as a dynamically produced bound state, and, if so, what its mass and couplings should be. The mass and couplings are determined by the self-consistency requirement that the bound state identified as A be the same as the A which enters as a force carrier, or as a constituent of the bound state.

An investigation of this kind, with the Σ (1193 MeV, $\frac{1}{2}^+$, $I=1$, $S=-1$) as guinea pig, is reported in this paper. The characteristics of the remaining baryons and mesons are taken from experiment, or, where experimental information is uncertain or nonexistent, are estimated theoretically and then varied in the computations. For a given set of assumptions about the other particles, the "input" Σ mass and couplings are varied in an ND^{-1} dynamical calculation until self-consistency between the "output" and "input" values is achieved.

Two aims motivate this work: first, to shed some light on the question of whether the Σ in particular is a composite object, hence on the question of whether all the strongly interacting particles are composite; secondly, but of equal importance, to see what happens when the matrix ND^{-1} method[1] is applied to a practical example involving several channels and many input forces.

The first thing to consider in constructing a dynamical model of the Σ is the question of what this particle would be made of, and what forces the constituents would feel. This is discussed in Sec. II. Section III summarizes the scattering theory and the ND^{-1} formalism on which the dynamical calculations are based, and treats the situation where a "force cut" overlaps the "unitarity cut" below physical threshold. The Born amplitudes representing the input forces are tabulated and commented upon in Sec. IV. Whether the input forces are attractive or repulsive is determined in Sec. V, which also explains some aspects of the plan for the dynamical calculations. The self-consistent results are

† Work supported in part by the U. S. Atomic Energy Commission, and in part by the National Science Foundation. This paper is based on a thesis submitted to the California Institute of Technology in partial fulfillment of the requirements for the degree of Doctor of Philosophy.

* Present address: Department of Physics, University of California, Berkeley, California.

[1] J. Bjorken, Phys. Rev. Letters 4, 473 (1960); and G. Chew and S. Mandelstam, Phys. Rev. 119, 467 (1960).